JACS
JOURNAL OF THE AMERICAN CHEMICAL SOCIETY
Article
pubs.acs.org/JACS

Cation-Dependent Gold Recovery with α-Cyclodextrin Facilitated by Second-Sphere Coordination

Zhichang Liu,[†] Avik Samanta,[†] Juying Lei,[‡] Junling Sun,[†] Yuping Wang,[†] and J. Fraser Stoddart*[,†]

[†]Department of Chemistry, Northwestern University, 2145 Sheridan Road, Evanston, Illinois 60208-3113, United States
[‡]School of Resources and Environmental Engineering, East China University of Science and Technology, 130 Meilong Road, Shanghai 200237, China

Supporting Information

ABSTRACT: Herein, we report an alkali metal cation-dependent approach to gold recovery, facilitated by second-sphere coordination with eco-friendly α-cyclodextrin (α-CD). Upon mixing eight salts composed of Na^+, K^+, Rb^+, or Cs^+ cations and $[AuX_4]^-$ (X = Cl/Br) anions with α-, β-, or γ-CD in water, co-precipitates form selectively from the three (out of 24) aqueous solutions containing α-CD with $KAuBr_4$, $RbAuBr_4$, and $CsAuBr_4$, from which the combination of α-CD and $KAuBr_4$ affords the highest yield. Single-crystal X-ray analyses reveal that in 20 of the 24 adducts CD and $[AuX_4]^-$ anions form 2:1 sandwich-type second-sphere adducts driven partially by [C−H···X−Au] interactions between $[AuX_4]^-$ anions and the primary faces of two neighboring CDs. In the adduct formed between α-CD and $KAuBr_4$, a $[K(OH_2)_6]^+$ cation is encapsulated inside the cavity between the secondary faces of two α-CDs, leading to highly efficient precipitation owing to the formation of a cation/anion alternating ion wire residing inside a continuous α-CD nanotube. By contrast, in the other 19 adducts, the cations are coordinated by OH groups and glucopyranosyl ring O atoms in CDs. The strong coordination of Rb^+ and Cs^+ cations by these ligands, in conjunction with the stereoelectronically favorable binding of $[AuBr_4]^-$ anions with two α-CDs, facilitates the co-precipitation of the two adducts formed between α-CD with $RbAuBr_4$ and $CsAuBr_4$. In order to develop an efficient process for green gold recovery, the co-precipitation yield of α-CD and $KAuBr_4$ has been optimized regarding both the temperature and the molar ratio of α-CD to $KAuBr_4$.

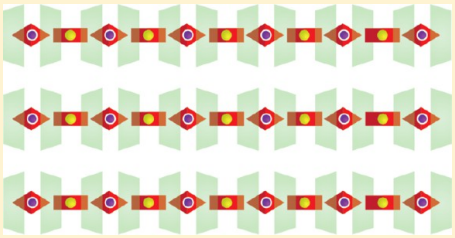

INTRODUCTION

Since the concept of second-sphere coordination—which relates to the noncovalent bonding interactions of chemical entities to the first coordination sphere of a transition metal complex—was first advanced[1] by Alfred Werner in 1912, investigations of its mechanisms of action and applications have emerged many decades later as a rapidly expanding area of research involving molecular recognition processes and self-assembly phenomena under the umbrellas of supramolecular[2] and host−guest[3] chemistry. Being driven[4] by noncovalent bonding interactions—including electrostatic,[5] hydrogen bonding,[6] van der Waals,[7] and charge transfer[8]—second-sphere coordination offers[9] potential advantages over covalent assembly, for instance (i) mild reaction conditions, (ii) good selectivity governing adduct formation based on very precise recognition between the metal complexes and the second-sphere ligands, and (iii) reversibility of the adduct formation. In this context, second-sphere coordination[10] between transition metal complexes and shape-persistent macrocyclic receptors—e.g., cyclodextrins[11] (CDs), crown ethers,[12] calixarenes,[13] cucurbiturils,[14] and cyclophanes[15]—has been recognized[16] as a promising route to the formation and the isolation of adducts. Although second-sphere coordination involving a number of transition metal complexes,[17] including those containing Cu,[12a,18] Fe,[19] Zn,[20] Co,[21] Ni,[7] Ir,[22] Ag,[23] Pt,[24] and Rh[21a,25] with a variety of macrocyclic and cage compounds, has long been investigated, second-sphere coordination of Au complexes was only recently discovered[26] serendipitously in relation to the recognition of square-planar tetrahaloaurate anions ($[AuX_4]^-$, X = Cl/Br) inside the cavities of α-, β-, and γ-CDs.

Our own recent research has revealed[27] that γ-CD can be linked by coordinating to one of several Group IA metal cations to form cyclodextrin metal−organic frameworks (CD-MOFs). During the screening of a wide range of anions, e.g., OH^-, CO_3^{2-}, F^-, Cl^-, Br^-, Ph_4B^-, $PhCO_2^-$, azobenzene-4,4′-dicarboxylate, etc., it transpired that, despite them being very different anions, in all cases, γ-CD and the alkali metal cations form isostructural highly porous, extended body-centered cubic structures with space group *I*432 and a unit cell edge of approximately 31 Å. For a time the nature of the anion accompanying the cation seemed to us to be unimportant. When the anions are $[AuX_4]^-$ (X = Cl/Br), however, we discovered serendipitously that γ-CD and the $[AuX_4]^-$ anions form solid-state superstructures whose crystals adopt a different, somewhat rare, highly symmetric tetragonal $P42_12$ space group wherein the $[AuX_4]^-$ anions are encapsulated between the primary (1°) faces of two γ-CD tori to form second-sphere adducts by means, inter alia, of [C−H···Br−Au] hydrogen bonding interactions. Much to our surprise, if

Received: May 15, 2016
Published: August 12, 2016

DOI: 10.1021/jacs.6b04986
J. Am. Chem. Soc. 2016, 138, 11643−11653

$KAuBr_4$ is used in combination with α-CD, the situation changes even more dramatically. When aqueous solutions of $KAuBr_4$ and α-CD at concentrations of 10 and 20 mM, respectively, are mixed, precipitation of needle-like crystals is observed within minutes.

Here, we report a systematic study of (i) the Group IA metal cation- and CD-dependent co-precipitation of $[AuX_4]^-$ (X = Cl/Br), (ii) the examination of the co-precipitates by both scanning electron microscopy (SEM) and powder X-ray diffraction (PXRD), (iii) the characterization of no less than 20 s sphere adducts between CDs ($\alpha/\beta/\gamma$) and $MAuX_4$ (M = Na/K/Rb/Cs and X = Cl/Br) by single-crystal XRD analysis, and (iv) the optimization of the yield of the co-precipitate between α-CD and $KAuBr_4$ as a function of different temperatures and absolute concentrations as well as the molar ratios of α-CD to $KAuBr_4$ in order to render the process more amenable to pilot-scale operation for gold recovery.

RESULTS AND DISCUSSION

Group IA Metal Cation- and CD-Dependent Co-precipitation of $[AuX_4]^-$ Anions. When aqueous solutions of each of $KAuCl_4$ and $KAuBr_4$ as well as aqueous solutions of α-, β-, and γ-CDs in turn are mixed, we observed that, after only a few minutes, the mixture of $KAuBr_4$ and α-CD leads to a pale brown co-precipitate, while all the other five mixtures remain as clear solutions in water. The co-precipitate was found to be composed of crystalline needles with high aspect ratios as characterized[26] by SEM. Atomic force microscopy (AFM) and single-crystal XRD analysis revealed that the solid-state superstructure is that of a one-dimensional (1D) second-sphere coordination polymer $\{[K(OH_2)_6][AuBr_4]\subset(\alpha\text{-CD})_2\}_n$—namely, a polymeric chain consisting of a 2:1 second-sphere adduct which is denoted as ***α*·K·Br** (a short-hand acronym which refers to CD·alkali metal cation·tetrahaloaurate anion)—which is generated from two first-sphere complex ions $[K(OH_2)_6]^+$ and $[AuBr_4]^-$ and two α-CD second-sphere ligands. The α-CD tori are stacked in the crystal and held together by [O−H···O] hydrogen bonds in a head-to-head and tail-to-tail alternating fashion to form 1D channels. The space between the OH groups on the secondary (2°) faces of repeating pairs of α-CDs acts as the first second-sphere cavity which is filled by a distorted octahedrally coordinated hexa-aqua K^+ cation ($[K(OH_2)_6]^+$). The square-planar $[AuBr_4]^-$ anion, which is oriented almost vertically, is encapsulated in the second second-sphere cavity between the primary (1°) OH faces of repeating face-to-face α-CD pairs, stabilized by [C−H···Br−Au] hydrogen bonding interactions. A seemingly perfect match in molecular recognition between α-CD, K^+, and $[AuBr_4]^-$ facilitates the specific second-sphere coordination involving both $[K(OH_2)_6]^+$ and $[AuBr_4]^-$ ions which interact with each other noncovalently so as to drive the co-precipitation of ***α*·K·Br**. The serendipitous discovery of the spontaneous co-precipitation of ***α*·K·Br** encouraged us to gain more insight into the recognition motifs behind the cooperative interactions between the CD tori and $MAuX_4$ by exploring the effects of (i) the diameters of the CD tori, (ii) the sizes and binding abilities of the alkali metal cations ($Na^+/K^+/Rb^+/Cs^+$), as well as (iii) the nature of the $[AuX_4]^-$ anions. Since α-CD has the smallest inner diameter of the three CDs and hence should be able to form more compact second-sphere adducts with $[AuX_4]^-$, we first of all examined all eight mixtures in water between $MAuX_4$ (M = Na/K/Rb/Cs and X = Cl/Br) and α-CD. Upon mixing aqueous solutions of $MAuX_4$ and α-CD in a 1:2 molar ratio, we observed that three—namely, $KAuBr_4$, $RbAuBr_4$, and $CsAuBr_4$—of the four $MAuBr_4$ salts form (Figure 1) brown co-precipitates with α-CD within a few minutes, while all the other five aqueous solutions, resulting from $NaAuBr_4$, and all four $MAuCl_4$ salts with α-CD remained clear. In striking contrast, no co-precipitation was observed in the case of the aqueous solutions of all 16 mixtures (in 1:2 molar ratios) of $MAuX_4$ and β- or γ-CD. These observations established the fact that only the salts composed of alkali metal cations and those larger than Na^+, along with $[AuBr_4]^-$, but not with $[AuCl_4]^-$, form co-precipitates with α-CD and not at all with β- or γ-CD. In order to quantify the efficiency of the co-precipitations of $[AuBr_4]^-$, UV−vis spectrophotometry was carried out with reference to the characteristic absorbance of $[AuBr_4]^-$ at around 380 nm to analyze the concentrations of $[AuBr_4]^-$ remaining in the filtrates. The results revealed (Figure 2) that at the concentrations of 10 mM in $MAuBr_4$ salts and 20 mM in α-CD, and at a temperature of 20 °C, $KAuBr_4$ produces the highest yield of 78%. $RbAuBr_4$ affords the lowest one of 41%, whereas $CsAuBr_4$ gives a modest yield of 68%—observations which indicate that the co-precipitation yields of $[AuBr_4]^-$ anions depend crucially on the nature of the alkali metal cation and that the K^+ ion is associated with the highest efficiency when it comes to the co-precipitation from aqueous solution of $[AuBr_4]^-$ anions. The selective removal of ^{135}Cs and ^{137}Cs from highly radioactive nuclear waste is a challenging task[13b,28] that has been met with only limited success to date. The co-precipitation of $CsAuBr_4$ with α-CD suggests another

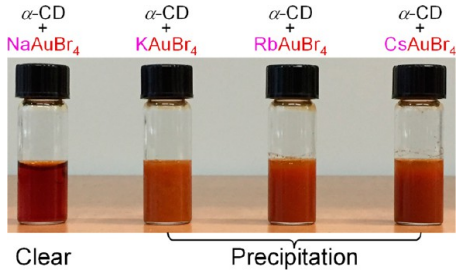

Figure 1. Cation-dependent co-precipitation of α-CD and $MAuBr_4$ (M = Na/K/Rb/Cs) in aqueous solutions. The concentrations of α-CD and $MAuBr_4$ are 20 and 10 mM, respectively.

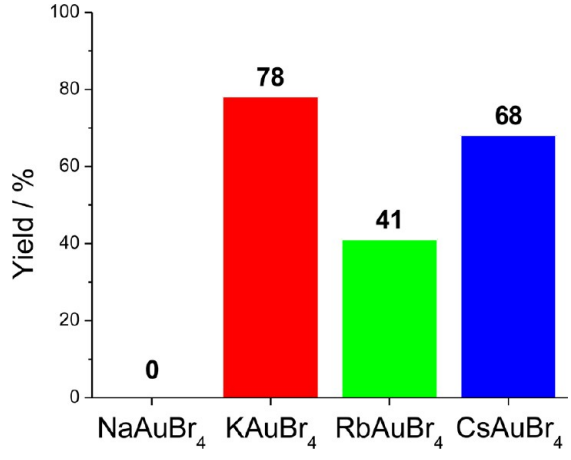

Figure 2. Yields of co-precipitates from four aqueous solutions of α-CD (20 mM) and $MAuBr_4$ (10 mM) (M = Na/K/Rb/Cs) measured at 20 °C by UV−vis spectrophotometry.

DOI: 10.1021/jacs.6b04986
J. Am. Chem. Soc. 2016, 138, 11643−11653

possible application which is the environmentally benign selective capture of Cs^+ from aqueous solution with relevance to the remediation of nuclear waste.

In order to gain further insight into this cation-dependent co-precipitation, SEM analyses on air-dried samples of the three co-precipitates obtained from aqueous solutions of $KAuBr_4$, $RbAuBr_4$, and $CsAuBr_4$ with α-CD—which are identified by the descriptors ***α*·K·Br**, ***α*·Rb·Br**, and ***α*·Cs·Br**—were carried out. SEM images reveal (Figure 3) that all three co-precipitates

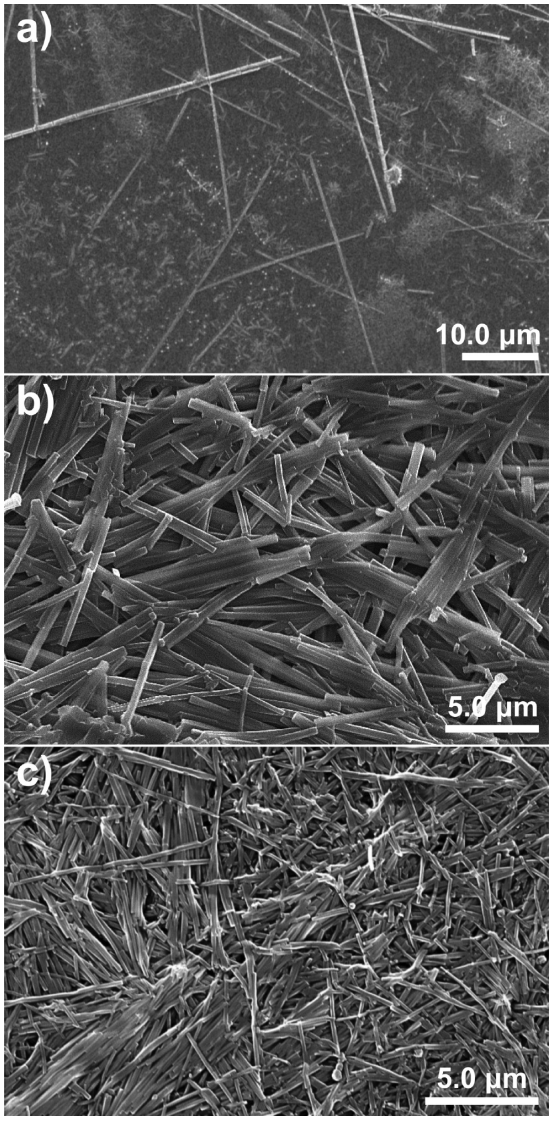

Figure 3. SEM images of three co-precipitated adducts. (a) The co-precipitate of ***α*·K·Br** composed of discrete high-aspect-ratio needle-like crystals. (b) The co-precipitate of ***α*·Rb·Br** composed of much thicker low-aspect-ratio needle-like crystals. (c) The co-precipitate of ***α*·Cs·Br** composed of thin needle-like crystals with moderate aspect ratios. Samples were prepared by drop-casting the as-synthesized co-precipitates onto silicon wafers, followed by drying in air.

constitute 1D needle-like crystals but with different diameters and aspect ratios. Among them, the co-precipitate of ***α*·K·Br** has diameters of 100−500 nm as well as very high aspect ratios reaching up to several hundreds, while the co-precipitate of ***α*·Cs·Br** has diameters of around 200 nm and aspect ratios extending up to 100. The co-precipitate of ***α*·Rb·Br** exhibits larger diameters (as high as 800 nm) with aspect ratios as low as 20. These observations show that the needles of ***α*·K·Br** and ***α*·Cs·Br**, which are obtained in high yields, have smaller diameters and higher aspect ratios, while the needles of ***α*·Rb·Br**, which are produced in a low yield, have a larger diameter and a lower aspect ratio.

X-ray Crystallography. In order to shed more light on the noncovalent bonding interactions driving these cation-dependent co-precipitations, XRD analyses were carried out on 20 single crystals. In the first instance, single crystals of all four adducts ***α*·Na·Br**, ***α*·K·Br**, ***α*·Rb·Br**, and ***α*·Cs·Br** between $MAuBr_4$ and α-CD which were suitable for X-ray crystallography were obtained by slow vapor diffusion of EtOH into dilute aqueous mixtures of $NaAuBr_4$, $KAuBr_4$, $RbAuBr_4$, and $CsAuBr_4$, respectively, containing α-CD. In all four solid-state superstructures (Figures 4a and 5), the ratios of $MAuBr_4$ to α-CD are 1:2. Although all four adducts have (Table 1) very similar unit cell parameters, ***α*·Na·Br** and ***α*·K·Br** adopt the same orthorhombic space group $P2_12_12$, while ***α*·Rb·Br** and ***α*·Cs·Br** exist in the same monoclinic $P2_1$ space group with β = 90.259(3)° for ***α*·Rb·Br** and 90.021(2)° for ***α*·Cs·Br**. In all four adducts, α-CD tori adopt an alternate head-to-head and tail-to-tail packing arrangement, forming 1D channels wherein the $[AuBr_4]^-$ anions are second-sphere coordinated in nearly collinear orientations (Figure 4a, $\phi < 10°$ and $\theta < 4°$) within the cavities between the primary (1°) faces of adjacent α-CD tori (**A** and **B**) by means of multiple [C−H···Br−Au] interactions involving the Br atoms and 12 H-5 and H-6 atoms on the 1° faces of the glucopyranosyl rings. Apparently, $[AuBr_4]^-$ anions act as linkers of two adjacent α-CD tori on account of the absence of significant [O−H···O] interactions between the 1° faces of α-CD tori. The striking differences among the four adducts are (i) the coordination environments of the alkali metal cations and hence (ii) the different linkages provided by these cations in the formation and co-precipitation of their superstructures. A unique situation arises (Figure 4a) in the case of ***α*·K·Br** wherein the K^+ cations are coordinated in their first sphere by six H_2O molecules to form equatorially distorted octahedral $[K(OH_2)_6]^+$ cations (mean K−O distance = 2.39 Å) which locate themselves in the second-sphere cavitand formed between the 2° faces of adjacent α-CD tori. This situation, to the best of our knowledge, is unique: generally speaking, the hydrophobic CD channels would prefer to encapsulate hydrophobic guests rather than the hydrophilic fully hydrated K^+ cations. In addition to acting as a guest, the $[K(OH_2)_6]^+$ cations also play the role of being linkers between two $[AuBr_4]^-$ anions by connecting them with [O−H···Br−Au] hydrogen bonding interactions (Br−O distances = 3.35(1) and 3.39(1) Å) between the *c*-axial H_2O molecules on the K^+ cations and Br atoms on the anions. As a consequence, a continuous polyionic chain—consisting of hydrogen-bonded $[K(OH_2)_6]^+$ and $[AuBr_4]^-$ ions lined up electrostatically in an alternating fashion—is second-sphere coordinated by the α-CD nanotube to form (Figure 5a) the compact cable-like superstructure of ***α*·K·Br**. By contrast, in the other three adducts ***α*·Na·Br**, ***α*·Rb·Br**, and ***α*·Cs·Br**, the metal cations are coordinated (Figure 4a) directly to the OH groups of the CD tori. In the case of ***α*·Na·Br**—which is the only adduct that does not precipitate—the Na^+ cations are evenly disordered over two sites on the 2° faces of α-CD tori, connecting adjacent tail-to-tail α-CD pairs along the *b*-axis to form (Figure 5b) 1D metal−organic superstructures by coordinating to four secondary OH groups (mean Na−O distance = 2.52 Å) from four α-CD tori. This observation suggests that the low-

DOI: 10.1021/jacs.6b04986
J. Am. Chem. Soc. 2016, 138, 11643−11653

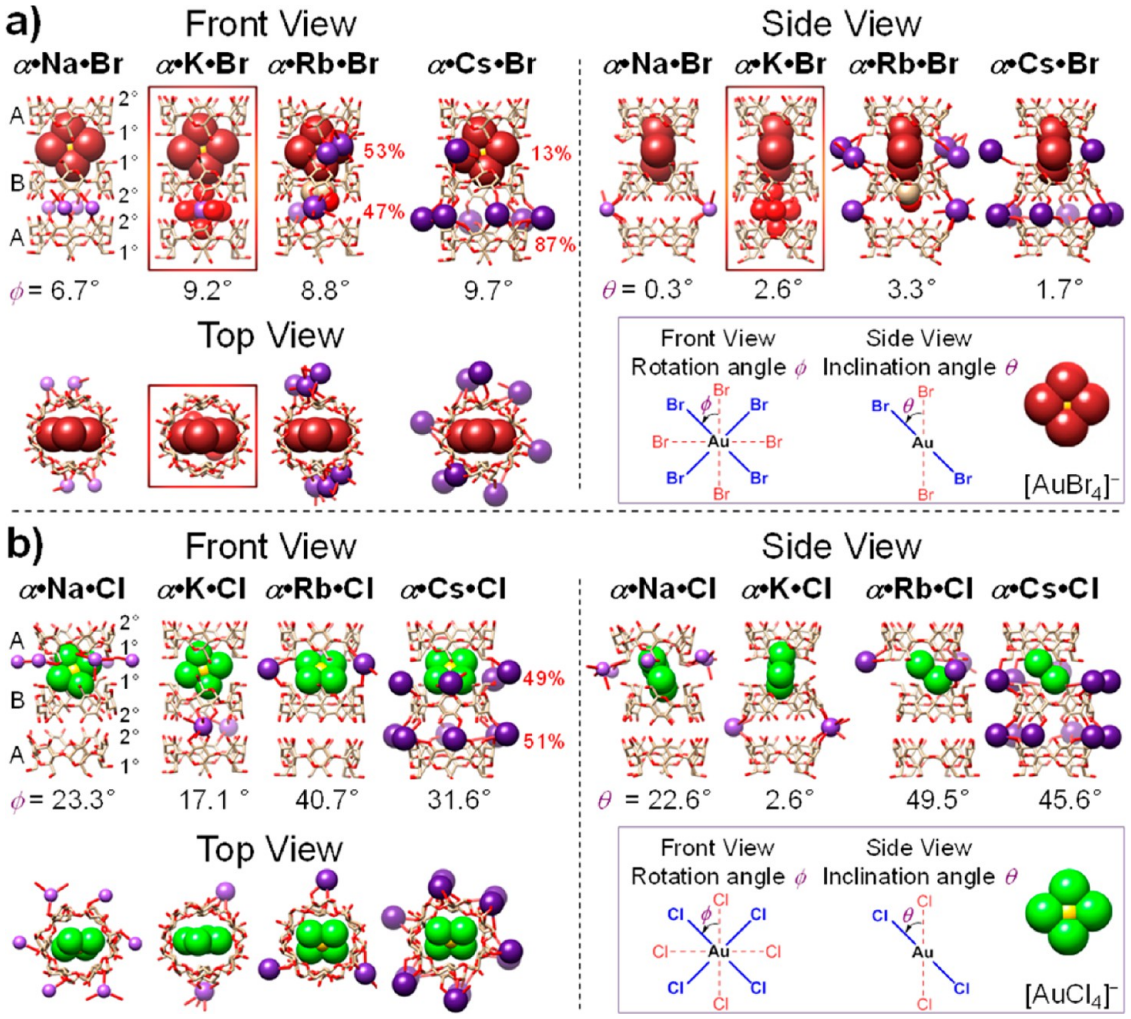

Figure 4. Single-crystal superstructures of all eight adducts formed between α-CD and $MAuX_4$ (M = Na/K/Rb/Cs, X = Cl/Br). (a) Three views (front, side, and top) of adducts ***α*·Na·Br**, ***α*·K·Br**, ***α*·Rb·Br**, and ***α*·Cs·Br**. (b) Three views (front, side, and top) of adducts ***α*·Na·Cl**, ***α*·K·Cl**, ***α*·Rb·Cl**, and ***α*·Cs·Cl**. The $[AuBr_4]^-$ and $[AuCl_4]^-$ anions, as well as the alkali metal cations, are represented in space-filling format. Appearing on the sides of the channels (front, side, and top), A and B indicate the differently oriented CD tori. 1° and 2° indicate the primary OH group and the secondary OH group faces, respectively. Occupancies of disordered Rb^+ and Cs^+ cations at the 1° and 2° faces are depicted in percentages in red. The rotation angle of the $[AuX_4]^-$ anion viewed from the front is defined as ϕ, and the inclination angle of the $[AuX_4]^-$ anion viewed from the side with respect to the central axis of the CD tori is defined as θ. Hydrogen atoms are omitted for the sake of clarity. C, tan; O, red; Br, brown; Cl, green; Au, yellow; Na, K, Rb, Cs, purple.

coordinating Na^+ cations might be unable to play a strong linking role at the 2° faces of adjacent α-CD pairs and so cooperate with the $[AuBr_4]^-$ anionic linkers located at the 1° faces and induce the co-precipitation of ***α*·Na·Br**. By contrast, the solid-state superstructures of the other two spontaneously co-precipitating adducts ***α*·Rb·Br** and ***α*·Cs·Br** indicate that both Rb^+ and Cs^+ cations are coordinated simultaneously to both the 1° and 2° faces of α-CD tori. In the case of ***α*·Rb·Br**, the Rb^+ cations are disordered over (i) two sites with a total occupancy of 53% at the 1° faces, connecting two head-to-head α-CD pairs by coordinating with three primary OH groups and two glucopyranosyl ring O atoms, and (ii) one site with an occupancy of 47% at the 2° faces, connecting two tail-to-tail α-CD pairs by coordinating to the seven secondary OH groups. This dual linking of the Rb^+ cations at the 1° and 2° faces results (Figure 5c) in a two-dimensional (2D) metal−organic network involving the b−c plane. It is composed of $[AuBr_4]^-$-encapsulated CD nanotubes arranged in parallel and linked by the Rb^+ cations. In the case of ***α*·Cs·Br**, the Cs^+ cations are (i) located mainly at the 2° faces with an occupancy of 87% and participate in connecting three triangularly arranged tail-to-tail α-CD pairs by coordinating (mean Cs−O distance = 3.17 Å) to nine secondary OH groups evenly from three α-CD pairs and (ii) located less significantly so at the 1° faces with an occupancy of 13% and coordinated (mean Cs−O distance = 3.08 Å) by three primary OH groups and one glucopyranosyl ring O atom. As a consequence, ***α*·Cs·Br** constitutes (Figure 5d) a three-dimensional (3D) metal−organic superstructure which is composed of $[AuBr_4]^-$-encapsulated parallel CD nanotubes linked in three dimensions by Cs^+ cations.

The analyses of the solid-state superstructures of the four adducts of α-CD and $MAuBr_4$ have led us to the conclusion that, although an excellent stereoelectronic fit between α-CD and $[AuBr_4]^-$ allows the anion to act out an indispensable linking role between the 1° faces of α-CD, the roles of the alkali metal cations are also crucial for the efficient formation and stabilization of the superstructure, leading to the spontaneous co-precipitation of an adduct. In the case of ***α*·K·Br**, the

DOI: 10.1021/jacs.6b04986
J. Am. Chem. Soc. 2016, 138, 11643−11653

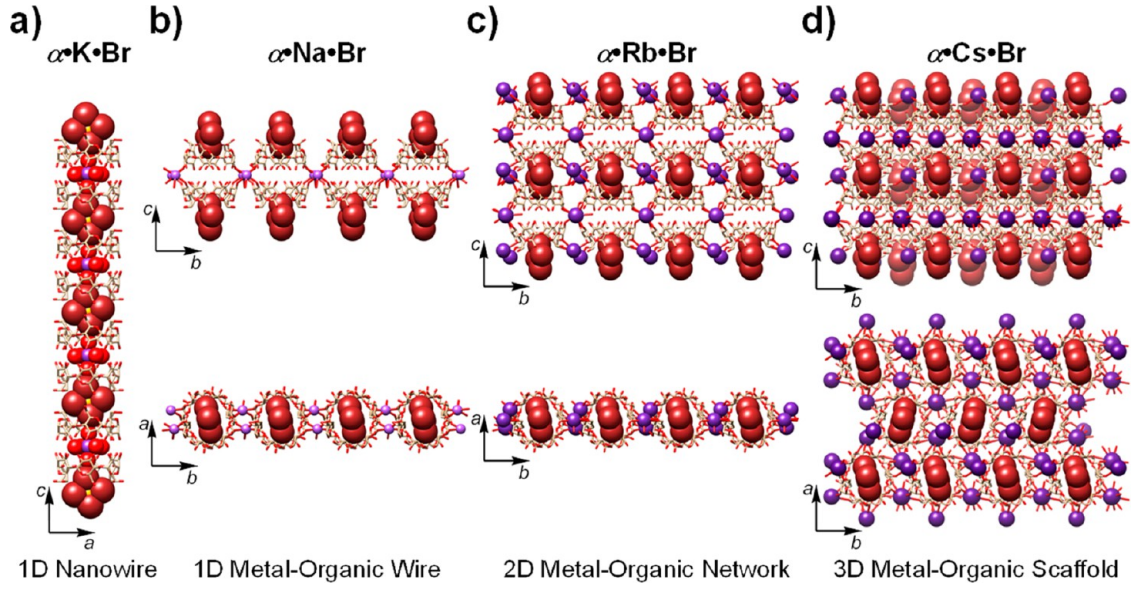

Figure 5. Single-crystal X-ray superstructures of the adducts (a) ***α*·K·Br**, (b) ***α*·Na·Br**, (c) ***α*·Rb·Br**, and (d) ***α*·Cs·Br**. The $[AuBr_4]^-$ anions and the alkali metal cations are represented in space-filling format. Hydrogen atoms are omitted for the sake of clarity. C, tan; O, red; Br, brown; Au, yellow; Na, K, Rb, Cs, purple.

Table 1. Crystallographic Data of Eight Complexes Formed between *α*-CD and $MAuX_4$ (M = Na/K/Rb/Cs, X = Cl/Br)

complex	***α*·Na·Br**	***α*·K·Br**	***α*·Rb·Br**	***α*·Cs·Br**	***α*·Na·Cl**	***α*·K·Cl**	***α*·Rb·Cl**	***α*·Cs·Cl**
CD:$MAuX_4$	2:1	2:1	2:1	2:1	2:1	2:1	2:1	2:1
T/K	100(2)	100(2)	100(2)	100(2)	100(2)	100(2)	100(2)	100(2)
crystal system	orthorhombic	orthorhombic	monoclinic	monoclinic	triclinic	monoclinic	monoclinic	monoclinic
space group	$P2_12_12$	$P2_12_12$	$P2_1$	$P2_1$	$P1$	$P2_1$	$P2_1$	$P2_1$
a/Å	23.7683(16)	23.7764(5)	23.6538(13)	23.6886(9)	13.6582(7)	23.6996(12)	23.8573(10)	23.8601(11)
b/Å	14.1475(9)	14.2049(6)	14.2585(8)	14.2587(6)	13.9202(7)	14.1860(8)	13.9510(5)	14.0483(6)
c/Å	16.2856(11)	16.3214(4)	16.3791(10)	16.3326(7)	15.6235(9)	16.2732(9)	16.0436(6)	15.9744(7)
α/°	90	90	90	90	93.585(2)	90	90	90
β/°	90	90	90.259(3)	90.021(2)	89.976(2)	90.041(4)	96.262(19)	96.309(15)
γ/°	90	90	90	90	118.8786(17)	90	90	90
V/Å^3	5476.2(6)	5512.4(3)	5524.1(5)	5516.6(4)	2594.4(2)	5471.1(5)	5308.0(4)	5322.1(4)
Z	2	2	2	2	1	2	2	2
ρ_{calcd}/g cm^{-3}	1.518	1.584	1.646	1.648	1.503	1.485	1.539	1.520
μ/mm^{-1}	5.125	5.469	5.671	7.558	3.954	1.585	5.010	7.026
F(000)	2544	2668	2788	2778	1220	2514	2532	2488
goodness-of-fit on F^2	1.073	1.129	1.074	1.033	1.046	0.987	1.028	1.050
R_1 [$I > 2\sigma(I)$]	0.0548	0.1072	0.0512	0.0580	0.0936	0.0674	0.0363	0.0611
wR_2 [all data]	0.1542	0.2817	0.1424	0.1583	0.2555	0.1867	0.0967	0.1651
CCDC no.	1479836	918412	1479838	1479849	1479837	918413	1479839	1479840

simultaneous second-sphere coordination of $[K(OH_2)_6]^+$ and $[AuBr_4]^-$ by *α*-CD tori, as well as the electrostatic interactions between the ion pairs, facilitate the highly efficient formation and aggregation of the unique 1D cable-like superstructures which lead to the rapid co-precipitation of ***α*·K·Br**. In the case of ***α*·Na·Br**, on account of the low coordination number of the Na^+ cation—resulting from its small ionic radius (0.97 Å)—these cations can only coordinate at the 2° faces of *α*-CD, forming 1D metal−organic wires which are unable to participate in the co-precipitation of ***α*·Na·Br**. By contrast, the larger ionic radii of Rb^+ (1.48 Å) and Cs^+ (1.67 Å) ions allow them to bridge more *α*-CD tori, forming a cross-linked 2D metal−organic network (***α*·Rb·Br**) and a 3D metal−organic superstructure (***α*·Cs·Br**) by coordinating simultaneously with more O atoms at the 1° and 2° faces, which—in cooperation with the linking of the $[AuBr_4]^-$ anions at the 1° faces of *α*-CD—facilitates the efficient formation and co-precipitation of the adducts ***α*·Rb·Br** and ***α*·Cs·Br**. We believe that the higher occupancy of the Cs^+ cation at the 2° faces, in addition to its nine-coordinate bridging to three *α*-CD pairs—compared to the occupancy of Rb^+ cation at the 2° faces and its seven-coordinate bridging to two *α*-CD pairs—results in the higher co-precipitation yield of ***α*·Cs·Br** when compared with that of ***α*·Rb·Br**.

In order to confirm that the nanostructures of the co-precipitates of ***α*·K·Br**, ***α*·Rb·Br**, and ***α*·Cs·Br** are in agreement with the superstructures present in the single crystals of these three adducts, filtered and air-dried samples were analyzed by powder XRD (PXRD). The experimental PXRD patterns (Figure 6) match very well with the simulated patterns based on the single-crystal X-ray data, an observation which confirms that the bulk co-precipitated phases of these adducts are

DOI: 10.1021/jacs.6b04986
J. Am. Chem. Soc. 2016, 138, 11643−11653

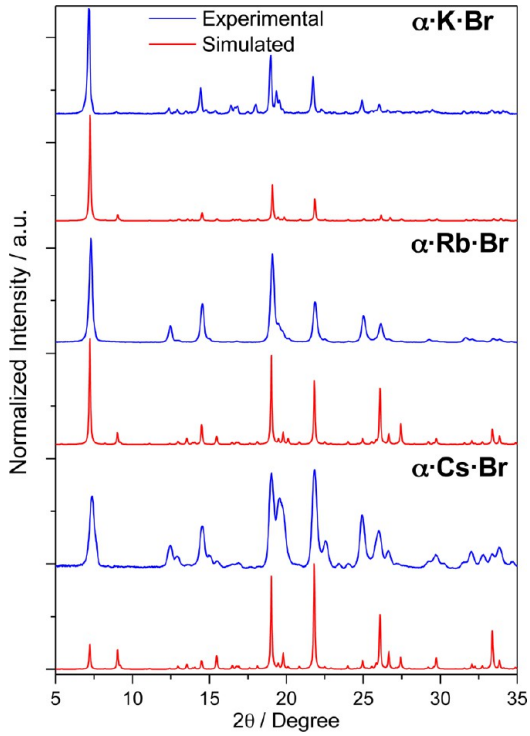

Figure 6. Powder X-ray diffraction patterns (blue traces) of the co-precipitated samples of (a) ***α*·K·Br**, (b) ***α*·Rb·Br**, and (c) ***α*·Cs·Br**, compared with the simulated patterns (red traces) derived from their crystal data.

ordered and that the nanostructures of the co-precipitates and the single crystals of the adducts are consistently identical.

In order to gain a better understanding of the mechanism of co-precipitation involving $[AuBr_4]^-$ and α-CD, single crystals of the four $[AuCl_4]^-$ adducts ***α*·Na·Cl**, ***α*·K·Cl**, ***α*·Rb·Cl**, and ***α*·Cs·Cl** were also obtained by employing a similar procedure (vapor diffusion of EtOH) to that described already from dilute aqueous solutions of α-CD and $MAuCl_4$ (M = Na/K/Rb/Cs), respectively, and subjected to single-crystal XRD analyses. All four adducts show (Figure 4b) a 1:2 ratio of $MAuCl_4$ to α-CD. Except for ***α*·Na·Cl**, which adopts (Table 1) a different triclinic *P*1 space group (Z = 1), the solid-state superstructures of ***α*·K·Cl**, ***α*·Rb·Cl**, and ***α*·Cs·Cl** are isostructural with those of ***α*·Rb·Br** and ***α*·Cs·Br**. In striking contrast to all adducts involving $MAuBr_4$ and α-CD, although the $[AuCl_4]^-$ anions are second-sphere coordinated within the cavity of the head-to-head α-CD dimer by means of [C−H···Cl−Au] interactions involving the Cl and H atoms on the 1° faces of the α-CD tori, the orientations of the $[AuCl_4]^-$ anions are much more tilted (Figure 4b, ϕ = 17.1−40.7° and θ = 2.6−49.5°) with respect to the axes of the nanotubes than those involving $[AuBr_4]^-$, presumably because the smaller $[AuCl_4]^-$ anions have to tilt that little bit more in order to maximize their [C−H···Cl−Au] interactions. This observation indicates that the size of the $[AuCl_4]^-$ anion does not match all that well with the α-CD tori and hence is not a good linker for α-CDs at their 1° faces. The alkali metal cations in all four $[AuCl_4]^-$ adducts are coordinated by OH groups and/or glucopyranosyl ring O atoms. In ***α*·Na·Cl**, 1D head-to-head and tail-to-tail α-CD nanotubes are arranged (Figures 4b and S1) in a *pseudo*-trigonal (β = 118.8(17)°) fashion in the a−b plane wherein the same-layer α-CDs (**A**)—rather than the complete **AB** pairs—are linked by the four-coordinate Na^+ cations at their 1° faces to form a 2D metal−organic layered superstructure by coordinating with three primary OH groups from three **A** α-CDs (plus one H_2O molecule), while the adjacent α-CD (**B**) layers are not coordinated by Na^+ cations. The solid-state superstructure (Figures 4b and S2) of ***α*·K·Cl** which is quite different from that of ***α*·K·Br**, is very similar to that of ***α*·Na·Br**. The bridging of the K^+ cations coordinated by the seven OH groups on the 2° faces of the α-CD dimers along the b-axis—rather than by 6 H_2O molecules encapsulated inside the CD cavity as in ***α*·K·Br**—gives (Figures 4b and S3) rise to the 1D metal−organic superstructures. This observation, in combination with the more tilted orientation (ϕ = 17.1°, Figure 4b, Front View) of the $[AuCl_4]^-$ anions, indicates that, although the K^+ cations could in principle form $[K(OH_2)_6]^+$ and find itself encapsulated inside the CD cavity, the $[AuCl_4]^-$ anion is too small to form the c-axial [O−H···Cl−Au] interactions with the $[K(OH_2)_6]^+$ cation, leading to an infinite polyionic chain inside the α-CD channel which is the sole reason for the high co-precipitation yield of ***α*·K·Br**. As a consequence, ***α*·K·Cl** is not co-precipitated spontaneously, while ***α*·K·Br** is co-precipitated quickly and efficiently. In the case of ***α*·Rb·Cl** (Figures 4b and S4), each Rb^+ cation bridges three head-to-head α-CD dimers by coordinating with five OH groups and two glucopyranosyl ring O atoms at the 1° faces to form a 2D metal−organic network in the a−b plane, while no coordinating interactions exist at the 2° faces. This 2D metal−organic network is oriented orthogonally to the α-CD channel and different from the one in ***α*·Rb·Br** which is parallel to the α-CD channel. The superstructure (Figures 4b and S5) of ***α*·Cs·Cl** is very similar to that of ***α*·Cs·Br**. The Cs^+ cations which are disordered with occupancies of 49% and 51% at the 1° and 2° faces, respectively, connect all the α-CD tori to form a 3D metal−organic scaffold. On comparing the solid-state superstructures of the four adducts between $MAuCl_4$ and α-CD with those of $MAuBr_4$ and α-CD, it can be concluded that, although alkali metal cations can bridge α-CD tori to form coordinated superstructures, the stereoelectronic match between the $[AuX_4]^-$ guest and the α-CD host is crucial for the occurrence of co-precipitation by these adducts, and only the $[AuBr_4]^-$ anion matches perfectly with α-CD to serve as a good linker for α-CD tori, a feature which, in cooperation with the alkali metal cations, facilitates the spontaneous co-precipitation of ***α*·K·Br**, ***α*·Rb·Br**, and ***α*·Cs·Br**.

In order to gain further insight into the influence of the size of the CD torus on the co-precipitation of $MAuX_4$ salts, the larger β- and γ-CDs have also been examined by mixing both CDs and the salts in H_2O. No co-precipitation, however, was observed in any of the 16 solutions. Single crystals of 12 adducts between β- and γ-CDs with $MAuX_4$ (M = Na/K/Rb and X = Cl/Br)—namely, ***β*·Na·Cl**, ***β*·K·Cl**, ***β*·Rb·Cl**, ***β*·Na·Br**, ***β*·K·Br**, ***β*·Rb·Br**, ***γ*·Na·Cl**, ***γ*·K·Cl**, ***γ*·Rb·Cl**, ***γ*·Na·Br**, ***γ*·K·Br**, and ***γ*·Rb·Br**—have been obtained and subjected to XRD analysis. The solid-state superstructures of the β-CD adducts are (Figure 7 and Table S1) isostructural with a 2:1 ratio of β-CD to $MAuX_4$ and adopt the monoclinic $P2_1$ space group, while the solid-state superstructures of the γ-CD adducts are (Figure 7 and Table S2) also isostructural with a 3:1 ratio of γ-CD to $MAuX_4$ and adopt the tetragonal $P42_12$ space group. In both the β- and γ-CD adducts, the $[AuX_4]^-$ anions are second-sphere coordinated inside the cavities between the 1° faces of two CD tori but with two different orientations—namely, a tilted one with ϕ = ∼ 42° and θ = 50° for the β-CD adducts

DOI: 10.1021/jacs.6b04986
J. Am. Chem. Soc. 2016, 138, 11643−11653

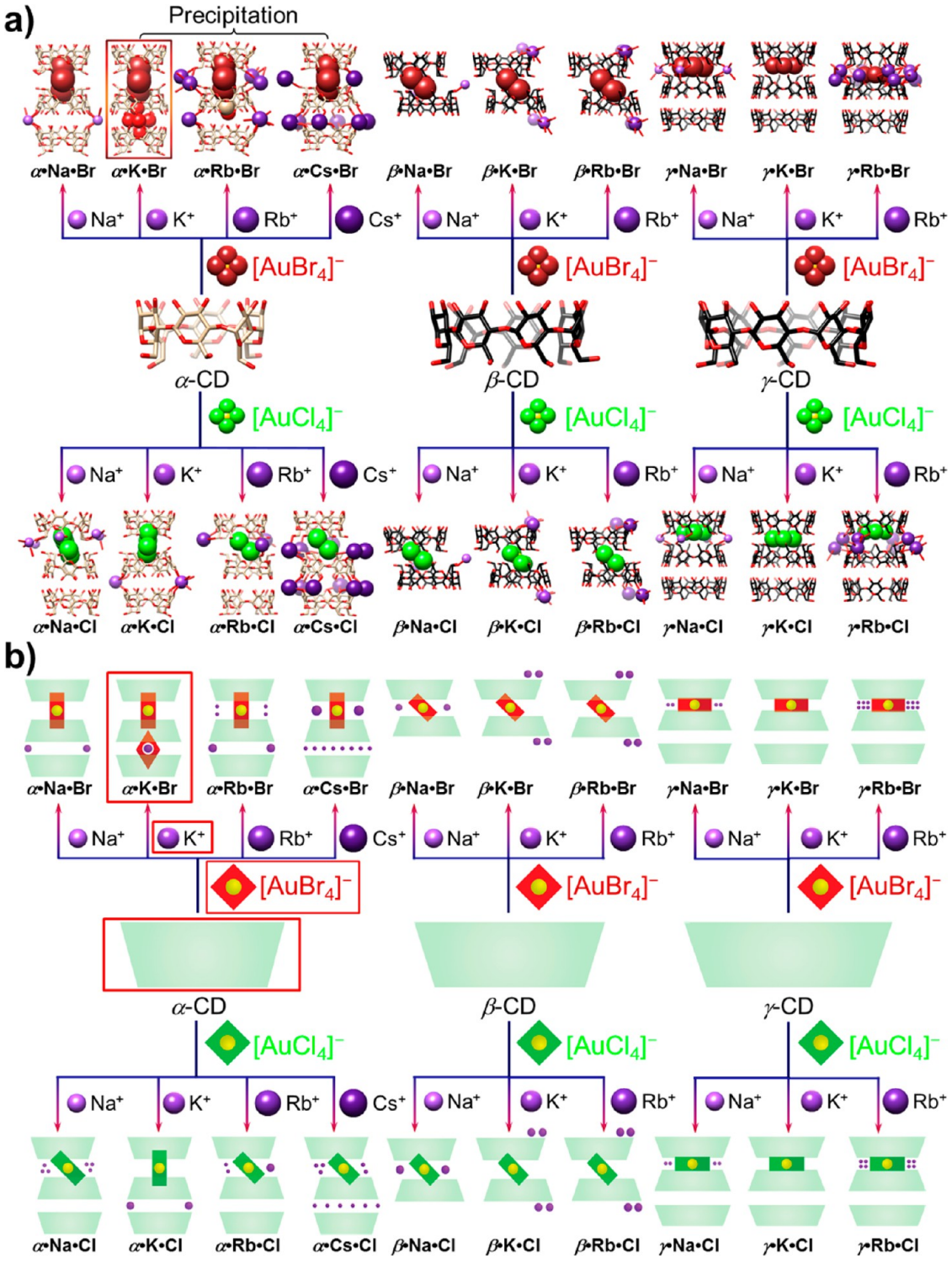

Figure 7. (a) Comparison of single-crystal X-ray superstructures of all 20 second-sphere coordination adducts—namely, ***α*·Na·Cl**, ***α*·K·Cl**, ***α*·Rb·Cl**, ***α*·Cs·Cl**, ***α*·Na·Br**, ***α*·K·Br**, ***α*·Rb·Br**, ***α*·Cs·Br**, ***β*·Na·Cl**, ***β*·K·Cl**, ***β*·Rb·Cl**, ***β*·Na·Br**, ***β*·K·Br**, ***β*·Rb·Br**, ***γ*·Na·Cl**, ***γ*·K·Cl**, ***γ*·Rb·Cl**, ***γ*·Na·Br**, ***γ*·K·Br**, and ***γ*·Rb·Br**. The $[AuBr_4]^-$ and $[AuCl_4]^-$ anions as well as the alkali metal cations are represented in space-filling format. C, tan for α-CD and black for β- and γ-CD; O, red; Br, brown; Cl, green; Au, yellow; Na, K, Rb, Cs, purple. Hydrogen atoms are omitted for the sake of clarity. (b) Schematic representations of the single-crystal X-ray superstructures of all 20 second-sphere coordination adducts in (a). Blue spheres indicate the alkali metal cations.

and a totally horizontal alignment with $\phi = 45°$ and $\theta = 90°$ in the case of the γ-CD adducts—ensuring multiple [C−H···X−Au] interactions with H atoms on the 1° faces of the γ-CD tori. The orientations of the $[AuX_4]^-$ anions in all the β- and γ-CD adducts are more tilted than those in the α-CD adducts, an observation which reveals a distinct trend—i.e., the larger the CD torus, the more tilted the orientation of the $[AuX_4]^-$ anions. The consistent trend for both $[AuCl_4]^-$ and $[AuBr_4]^-$ in β- and γ-CD adducts suggests that (i) the subtle differences between the $[AuCl_4]^-$ and $[AuBr_4]^-$ anions no longer lead to

DOI: 10.1021/jacs.6b04986
J. Am. Chem. Soc. 2016, 138, 11643−11653

significant changes in solid-state superstructures and (ii) the more tilted orientations for both anions result from the larger CD tori limiting their ability to serve as steric matching linkers of the CD tori in the formation of compact solid-state superstructures which are a prerequisite for the co-precipitation of the adducts. In contrast with the different coordination geometries of the cations, in the case of all the α-CD adducts, the alkali metal cations in β- and γ-CD adducts adopt (Figure 7) the same coordination geometries and locate themselves at the same coordination sites. In the case of β-CD adducts, only the Na^+ cations in ***β*·Na·Br** and ***β*·Na·Cl** are coordinated between the 1° faces of β-CD, while the K^+ and Rb^+ cations in ***β*·K·Br**, ***β*·K·Cl**, ***β*·Rb·Br**, and ***β*·Rb·Cl** are coordinated at the 2° faces of β-CD. In the case of γ-CD adducts, although the Na^+, K^+, and Rb^+ cations are disordered over several sites and their coordination numbers are different, all of them are coordinated at the 1° faces of the γ-CD tori.

On the basis of systematic X-ray diffraction analyses of the single-crystal solid-state superstructures carried out on these 20 adducts, we can conclude that the spontaneous co-precipitation of the CD with $MAuX_4$ is determined by (i) a stereoelectronic fit between $[AuX_4]^-$ and the CD torus which facilitates the formation of the compact second-sphere coordination adducts of $[AuX_4]^-$ and the CD, in cooperation with (ii) the bridging by the alkali metal cations. On account of these two factors, the adducts can be classified into three categories: (i) co-precipitated adducts, namely, ***α*·K·Br**, ***α*·Rb·Br**, and ***α*·Cs·Br**, resulting from good stereoelectronic matches between $[AuBr_4]^-$ and α-CD in cooperation with the connecting or bridging by K^+, Rb^+, and Cs^+ cations; (ii) the nonprecipitated adduct ***α*·Na·Br** as a result of the weak coordination of Na^+; and (iii) the remaining nonprecipitated adducts because of the poor stereoelectronic matches between $[AuX_4]^-$ and CD. In the first category, the best stereoelectronic match between $[AuBr_4]^-$ and α-CD, in cooperation with the encapsulation of $[K(OH_2)_6]^+$, leads to a unique alternating polyionic chain, second-sphere coordinated by α-CD nanotubes which result in the highest co-precipitation yield for ***α*·K·Br**, heralding a promising strategy for gold recovery by means of second-sphere coordination, making use of α-CD—an environmentally benign and inexpensive carbohydrate.

Optimization of the Co-precipitation Yield of *α*·K·Br. Given the potential applications of ***α*·K·Br** to eco-friendly gold recovery, the yield of the co-precipitate of ***α*·K·Br** was optimized with respect to temperature and the molar ratio of α-CD to $KAuBr_4$. An aqueous solution of α-CD (20 mM) and $KAuBr_4$ (10 mM) was prepared by dissolving $KAuBr_4$ in H_2O, followed by adding α-CD as a powder. Five identical portions of this solution were immersed in water baths at five preset temperatures (0, 4, 10, 15, and 20 °C) for 10 h. The resulting mixtures, consisting of pale-brown suspensions, were filtered, and the concentrations of the $[AuBr_4]^-$ anion remaining in the filtrates were analyzed by UV−vis spectrophotometry. On account of the fact that the filtrates at different temperatures are already saturated aqueous solutions of the ***α*·K·Br** adduct, the concentrations of ***α*·K·Br** in the filtrates obtained by UV−vis spectrophotometry represent the solubilities of ***α*·K·Br** at different temperatures. UV−vis spectrophotometry reveals that the aqueous solubility of ***α*·K·Br** changes (Figure 8, blue line) from 2.20 to 0.63 mM upon decreasing the crystallization temperature from 20 to 0 °C, an observation which indicates that the lower the temperature, the lower the solubility of the adduct. On the basis of the initial and residual concentrations of

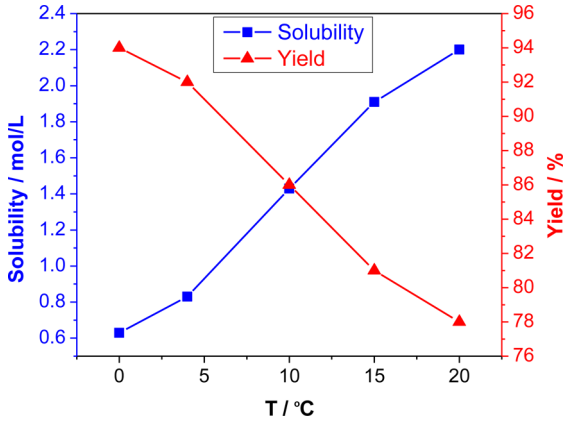

Figure 8. Effect of changes in temperature on the yield (red trace) and solubility (blue trace) of the co-precipitated complex ***α*·K·Br**. The initial concentration of $KAuBr_4$ is 10 mM.

***α*·K·Br** in aqueous solutions, the yields of the co-precipitated adduct at different temperatures can be calculated. Upon decreasing the temperature from 20 to 0 °C, the yields of the co-precipitated ***α*·K·Br** increase (Figure 8, red line) from 78 to 94%, an observation which indicates that the lower the temperature, the more efficient the co-precipitation process. On the basis of these profiles of solubilities and yields with temperatures, it can be concluded that (i) higher initial concentrations of $KAuBr_4$ and (ii) lower crystallization temperatures lead to the higher yields of the co-precipitated ***α*·K·Br** adduct. We believe that 0 °C is a practically operable temperature for the co-precipitation of ***α*·K·Br** on account of the accessibility of ice−water baths.

Despite the 1:2 ratio of $KAuBr_4$ to α-CD in ***α*·K·Br** having been unambiguously confirmed by single-crystal XRD analysis, the question as to whether the change in the ratio of $KAuBr_4$ to α-CD might influence the yield of the co-precipitate of ***α*·K·Br** still needs to be investigated from an economic point of view. Five aqueous solutions of α-CD and $KAuBr_4$ (10 mM), corresponding to the molar ratios of 1:1, 1:2, 1:3, 1:4, and 1:5 of $KAuBr_4$ to α-CD, were prepared. The 1:1 mixture became clear in 10 s and turned milky after 1 h, while the 1:2 mixture became clear for about 1 min and then gradually turned milky. By contrast, 1:3, 1:4, and 1:5 mixtures became milky in 10 s. These mixtures were then immersed into a water bath at 20 °C for 10 h. The mixtures, which consist of pale-brown suspensions, were filtered, and the concentrations of the $[AuBr_4]^-$ anion remaining in the filtrates were analyzed by UV−vis spectrophotometry. The yields of the co-precipitates of the different samples were obtained on the basis of the initial and residual concentrations of the $[AuBr_4]^-$ anion in the aqueous solutions. UV−vis spectrophotometry reveals (Figure 9) that the 1:1 mixture affords the lowest yield (32%) of ***α*·K·Br**, while the 1:2, 1:3, 1:4, and 1:5 mixtures give very similar yields (78% for 1:2/77% for 1:3/83% for 1:4/80% for 1:5) corresponding to an average yield of 80%. These results indicate that, upon increasing the amount of α-CD after reaching a 1:2 molar ratio of $KAuBr_4$ to α-CD, the yield of the co-precipitated adduct remains constant. On the basis of the identical yields obtained from 1:2, 1:3, 1:4, and 1:5 mixtures, it can be concluded that the co-precipitated adduct ***α*·K·Br** has the constant composition of 1:2 for $KAuBr_4$ to α-CD, an observation which is consistent with the single-crystal X-ray superstructure of ***α*·K·Br**. Thus, the yield cannot be further

DOI: 10.1021/jacs.6b04986
J. Am. Chem. Soc. 2016, 138, 11643−11653

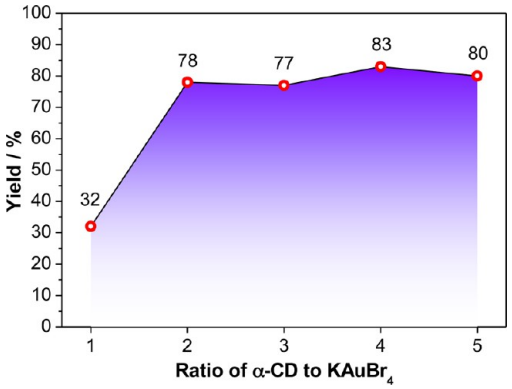

Figure 9. Effect of changes in ratio of α-CD to $KAuBr_4$ on the yield of the co-precipitated complex ***α*·K·Br**. The initial concentrations of $KAuBr_4$ in all five aqueous solutions are 10 mM.

enhanced by increasing the concentration of α-CD after reaching a 1:2 molar ratio of $KAuBr_4$ to α-CD, whereas it decreases if the ratio is lower than 1:2.

^{1}H and DOSY NMR Spectroscopies. In order to probe the mechanism of the supramolecular polymerization of ***α*·K·Br**, ^{1}H NMR titrations were performed by adding small volumes of a concentrated aqueous solution (41.80 mM) of $KAuBr_4$ in D_2O into a solution (1.18 mM) of α-CD in D_2O. ^{1}H NMR titration spectra reveal (Figure S6) that, despite changing the molar ratios of $KAuBr_4$ to α-CD from 0:1 to 3.55:1, no significant alterations in the chemical shifts of the resonances of the protons on α-CD were evident, an observation which indicates that, at these ranges of concentrations and molar ratios, any assembly between α-CD and $[AuBr_4]^-$ cannot be detected by ^{1}H NMR spectroscopy. In order to investigate the dynamics of formation of ***α*·K·Br**, we carried out variable-temperature (VT) ^{1}H NMR spectroscopy on a saturated solution (2.20 mM at 20 °C) of ***α*·K·Br** in D_2O. The VT ^{1}H NMR spectra show (Figure S7) that no large differences in the chemical shifts of the α-CD protons are observed, even though the temperature is decreased from 95 to 5 °C and a suspension appears in the solution at 5 °C. For comparison, VT ^{1}H NMR spectra (Figure S8) of a solution of α-CD at the same concentration of 2.20 mM were recorded over a range of temperatures from 25 to 5 °C. No perceptible changes in the chemical shifts of the α-CD protons were observed, suggesting that the chemical shifts of the α-CD protons are not influenced in D_2O, even in the absence of $KAuBr_4$. These observations indicate that most likely no significant assembly and aggregation between α-CD and $KAuBr_4$ occurs in the solution phase. In order to confirm that there is no significant assembly of α-CD and $KAuBr_4$ even in saturated solution, DOSY NMR spectroscopy was performed on a saturated solution (2.20 mM) of ***α*·K·Br** and a solution of α-CD at the same concentrations. DOSY NMR spectra of both these samples show (Figure S9) identical diffusion coefficients (D) of 3.98×10^{-10} m^2 s^{-1}. The consistency between the D values of two samples suggests that the existence of $KAuBr_4$ does not lead to changes of the aggregation state of α-CD in the aqueous solution phase. This observation indicates that the co-precipitation of α-CD and $KAuBr_4$ could be the result of cooperative crystallization, triggered by the synergetic second-sphere coordination between the stereoelectronically matched guests $[AuBr_4]^-$ and $[K(OH_2)_6]^+$ with the host α-CD, which is undetectable on the ^{1}H NMR time scale by DOSY experiments, presumably because of the rapid dynamic exchange of the species in solution.

CONCLUSIONS

In summary, we have presented in this full paper a systematic investigation of the serendipitous discovery of the alkali metal cation-selective and cyclodextrin-dependent co-precipitation of the square-planar anions $[AuX_4]^-$ (X = Cl/Br) in aqueous solution. From among 24 aqueous mixtures examined involving α-, β-, γ-CDs, and $MAuX_4$ (M = Na/K/Rb/Cs, X = Cl/Br), co-precipitation occurs selectively from only three aqueous solutions—those of α-CD with $KAuBr_4$, $RbAuBr_4$, and $CsAuBr_4$—while the mixture of α-CD and $KAuBr_4$ gives the fastest and highest co-precipitation yield by far. All three co-precipitates were found by scanning electron microscopy and powder X-ray diffraction analysis to possess crystalline needle-like nanostructures. The crystalline superstructures of 20 adducts formed between α-, β-, γ-CDs, and $MAuX_4$ were characterized by single-crystal XRD to be 2:1 sandwich-type second-sphere adducts of the CD hosts and the $[AuX_4]^-$ guests, stabilized by multiple [C−H···X−Au] interactions between the $[AuX_4]^-$ anions and the primary faces of two CD tori. The occurrence of the spontaneous co-precipitation of the CD and $MAuX_4$ salts relies on (i) the stereoelectronic matches between the square-planar $[AuX_4]^-$ anions and the CD tori, which leads to the formation of the stable 2:1 second-sphere crystalline adducts of $[AuX_4]^-$ and two CD tori, in conjunction with (ii) the bridging of the alkali metal cations between these pairs of CD tori. Good stereoelectronic matches between the $[AuBr_4]^-$ anions and the α-CD tori, with assistance from the strong connecting roles provided by the K^+, Rb^+, and Cs^+ cations, results in the highly selective co-precipitations of ***α*·K·Br**, ***α*·Rb·Br**, and ***α*·Cs·Br**. In particular, the most efficient co-precipitation yield involving ***α*·K·Br** can be ascribed to its unique 1D cable-like superstructure which is constituted of an infinite array of $[K(OH_2)_6]^+$ and $[AuBr_4]^-$ arranged alternately in ion wires encapsulated by head-to-head and tail-to-tail α-CD tori, generating nanotubes driven by the cooperative dual second-sphere coordination of $[K(OH_2)_6]^+$ and $[AuBr_4]^-$ inside the cavities between the secondary and primary faces, respectively, of the CD tori. By contrast, in all other adducts, the alkali metal cations are coordinated by OH groups and glucopyranosyl ring O atoms in the CD tori. The geometrically favorable second-sphere coordination of $[AuBr_4]^-$ and two α-CDs, in cooperation with the strong binding of both Rb^+ and Cs^+ cations to OH groups and glucopyranosyl ring O atoms, facilitates the co-precipitation of ***α*·Rb·Br** and ***α*·Cs·Br**. The yield of the co-precipitate of ***α*·K·Br** has been optimized in relation to temperature and molar ratios of α-CD to $KAuBr_4$ in an effort to make the process more amenable to the pilot-scale operation for gold recovery.

Gold recovery using environmentally friendly and sustainable chemical processes is a need of overriding importance in today's world.[29] For over a century, gold extraction has relied[30] upon the use of sodium cyanide and mercury as the chief reagents for extracting gold from ore. Cyanidation is used[31] in 83% of gold production with most of that remaining employing mercury. Cyanide is highly toxic and can be fatal to humans and animals if ingested in even small quantities.[29] Because of its toxicity, sodium cyanide has already been banned[32] in some countries, and it is becoming difficult in other countries to obtain the rights to use the cyanide technology. Moreover, serious environmental pollution and human health hazards are

DOI: 10.1021/jacs.6b04986
J. Am. Chem. Soc. 2016, 138, 11643−11653

created[33] by smaller-scale miners using mercury. In addition to gold mining, a new market, often referred[34] to as "urban mining", has emerged in recent years with the growth of the electronic industry since gold is used extensively in the manufacture of smart phones and computers. The results of this in-depth investigation demonstrate the enormous potential of this unprecedented and highly selective co-precipitation of environmentally benign α-CD and $KAuBr_4$ for green gold recovery, which is required if we are to avoid the use of toxic cyanide salts and mercury commonly employed in the current mining and recovery of gold.

■ ASSOCIATED CONTENT

Supporting Information

. The Supporting Information is available free of charge on the ACS Publications website at DOI: 10.1021/jacs.6b04986.

Detailed information regarding the experimental methods and procedures, X-ray crystallographic data, and supporting figures and tables (PDF)

CIF files for α·Na·Br, α·Rb·Br, α·Cs·Br, α·Na·Cl, α·Rb·Cl, α·Cs·Cl, β·Na·Br, β·Rb·Br, β·Na·Cl, β·Rb·Cl, γ·Na·Br, γ·Rb·Br, γ·Na·Cl, and γ·Rb·Cl

■ AUTHOR INFORMATION

Corresponding Author

*stoddart@northwestern.edu

Notes

The authors declare no competing financial interest.

■ ACKNOWLEDGMENTS

We thank Dr Roger Pettman for his useful suggestions and helpful discussions. We thank Drs. Charlotte L. Stern and Amy A. Sarjeant for carrying out the single-crystal XRD analyses. This work made use of the EPIC facility of the NUANCE Center at Northwestern University, which has received support from the Soft and Hybrid Nanotechnology Experimental (SHyNE) Resource (NSF NNCI-1542205); the MRSEC program (NSF DMR-1121262) at the Materials Research Center; the International Institute for Nanotechnology (IIN); and the State of Illinois, through the IIN.

■ REFERENCES

(1) (a) Werner, A. *Ber. Dtsch. Chem. Ges.* **1912**, *45*, 121. (b) Liu, Z.; Schneebeli, S. T.; Stoddart, J. F. *Chimia* **2014**, *68*, 315.

(2) Lehn, J.-M. *Angew. Chem., Int. Ed. Engl.* **1988**, *27*, 89.

(3) Cram, D. J. *Angew. Chem., Int. Ed. Engl.* **1988**, *27*, 1009.

(4) Busschaert, N.; Caltagirone, C.; Van Rossom, W.; Gale, P. A. *Chem. Rev.* **2015**, *115*, 8038.

(5) (a) Liu, Y.; Hu, C.; Comotti, A.; Ward, M. D. *Science* **2011**, *333*, 436. (b) Kaphan, D. M.; Levin, M. D.; Bergman, R. G.; Raymond, K. N.; Toste, F. D. *Science* **2015**, *350*, 1235.

(6) (a) Taylor, R.; Kennard, O. *J. Am. Chem. Soc.* **1982**, *104*, 5063. (b) Steed, J. W.; McCool, B. J.; Junk, P. C. *J. Chem. Soc., Dalton Trans.* **1998**, 3417. (c) Beauchamp, D. A.; Loeb, S. J. *Chem. - Eur. J.* **2002**, *8*, 5084.

(7) Atwood, J. L.; Orr, G. W.; Hamada, F.; Vincent, R. L.; Bott, S. G.; Robinson, K. D. *J. Am. Chem. Soc.* **1991**, *113*, 2760.

(8) Foster, R. *Organic Charge-Transfer Complexes*; Academic Press: New York, 1969.

(9) Wilson, A. M.; Bailey, P. J.; Tasker, P. A.; Turkington, J. R.; Grant, R. A.; Love, J. B. *Chem. Soc. Rev.* **2014**, *43*, 123.

(10) (a) Colquhoun, H. M.; Stoddart, J. F.; Williams, D. J. *Angew. Chem., Int. Ed. Engl.* **1986**, *25*, 487. (b) Stoddart, J. F.; Zarzycki, R. *Rec. Trav. Chim. Pays-Bas* **1988**, *107*, 515. (c) Raymo, F. M.; Stoddart, J. F. *Chem. Ber.* **1996**, *129*, 981.

(11) (a) Wenz, G. *Angew. Chem., Int. Ed. Engl.* **1994**, *33*, 803. (b) Wenz, G.; Han, B.-H.; Müller, A. *Chem. Rev.* **2006**, *106*, 782. (c) Hapiot, F.; Tilloy, S.; Monflier, E. *Chem. Rev.* **2006**, *106*, 767. (d) Harada, A.; Takashima, Y.; Nakahata, M. *Acc. Chem. Res.* **2014**, *47*, 2128.

(12) (a) Colquhoun, H. M.; Lewis, D. F.; Stoddart, J. F.; Williams, D. J. *J. Chem. Soc., Dalton Trans.* **1983**, 607. (b) Steed, J. W. *Coord. Chem. Rev.* **2001**, *215*, 171.

(13) (a) Atwood, J. L.; Barbour, L. J.; Hardie, M. J.; Raston, C. L. *Coord. Chem. Rev.* **2001**, *222*, 3. (b) Wintergerst, M. P.; Levitskaia, T. G.; Moyer, B. A.; Sessler, J. L.; Delmau, L. H. *J. Am. Chem. Soc.* **2008**, *130*, 4129. (c) Kim, S. K.; Sessler, J. L. *Acc. Chem. Res.* **2014**, *47*, 2525.

(14) (a) Kim, S.-Y.; Jung, I.-S.; Lee, E.; Kim, J.; Sakamoto, S.; Yamaguchi, K.; Kim, K. *Angew. Chem., Int. Ed.* **2001**, *40*, 2119. (b) Lagona, J.; Mukhopadhyay, P.; Chakrabarti, S.; Isaacs, L. *Angew. Chem., Int. Ed.* **2005**, *44*, 4844. (c) Kim, K.; Selvapalam, N.; Ko, Y. H.; Park, K. M.; Kim, D.; Kim, J. *Chem. Soc. Rev.* **2007**, *36*, 267. (d) Barrow, S. J.; Kasera, S.; Rowland, M. J.; del Barrio, J.; Scherman, O. A. *Chem. Rev.* **2015**, *115*, 12320.

(15) Ashton, P. R.; Claessens, C. G.; Hayes, W.; Stoddart, J. F.; Menzer, S.; White, A. J. P.; Williams, D. J. *Angew. Chem., Int. Ed. Engl.* **1995**, *34*, 1862.

(16) Mercer, D. J.; Loeb, S. J. *Chem. Soc. Rev.* **2010**, *39*, 3612.

(17) Thuéry, P. *Inorg. Chem.* **2010**, *49*, 9078.

(18) Li, L.; Tong, J.; Guo, F.; Marti-Rujas, J. *CrystEngComm* **2016**, *18*, 2284.

(19) (a) Harada, A.; Takahashi, S. *J. Chem. Soc., Chem. Commun.* **1984**, 645. (b) Klingert, B.; Rihs, G. *Organometallics* **1990**, *9*, 1135. (c) Dalrymple, S. A.; Parvez, M.; Shimizu, G. K. H. *Chem. Commun.* **2001**, 2672. (d) Zhuge, F.; Wu, B.; Yang, J.; Janiak, C.; Tang, N.; Yang, X.-J. *Chem. Commun.* **2010**, *46*, 1121. (e) Nakahata, M.; Takashima, Y.; Yamaguchi, H.; Harada, A. *Nat. Commun.* **2011**, *2*, 511.

(20) (a) Turkington, J. R.; Cocalia, V.; Kendall, K.; Morrison, C. A.; Richardson, P.; Sassi, T.; Tasker, P. A.; Bailey, P. J.; Sole, K. C. *Inorg. Chem.* **2012**, *51*, 12805. (b) Riddell, I. A.; Ronson, T. K.; Nitschke, J. R. *Chem. Sci.* **2015**, *6*, 3533.

(21) (a) Klingert, B.; Rihs, G. *J. Inclusion Phenom. Mol. Recognit. Chem.* **1991**, *10*, 255. (b) Reddy, D. S.; Duncan, S.; Shimizu, G. K. H. *Angew. Chem., Int. Ed.* **2003**, *42*, 1360.

(22) Colquhoun, H. M.; Stoddart, J. F.; Williams, D. J. *J. Am. Chem. Soc.* **1982**, *104*, 1426.

(23) Kohyama, Y.; Murase, T.; Fujita, M. *Angew. Chem., Int. Ed.* **2014**, *53*, 11510.

(24) (a) Alston, D. R.; Lilley, T. H.; Stoddart, J. F. *J. Chem. Soc., Chem. Commun.* **1985**, 1600. (b) Alston, D. R.; Slawin, A. M. Z.; Stoddart, J. F.; Williams, D. J. *J. Chem. Soc., Chem. Commun.* **1985**, 1602. (c) Alston, D. R.; Slawin, A. M. Z.; Stoddart, J. F.; Williams, D. J.; Zarzycki, R. *Angew. Chem., Int. Ed. Engl.* **1988**, *27*, 1184. (d) Harada, A.; Yamamoto, S.; Takahashi, S. *Organometallics* **1989**, *8*, 2560. (e) Alston, D. R.; Ashton, P. R.; Lilley, T. H.; Stoddart, J. F.; Zarzycki, R.; Slawin, A. M. Z.; Williams, D. J. *Carbohydr. Res.* **1989**, *192*, 259. (f) Bell, K. J.; Westra, A. N.; Warr, R. J.; Chartres, J.; Ellis, R.; Tong, C. C.; Blake, A. J.; Tasker, P. A.; Schröder, M. *Angew. Chem., Int. Ed.* **2008**, *47*, 1745.

(25) Alston, D. R.; Slawin, A. M. Z.; Stoddart, J. F.; Williams, D. J. *Angew. Chem., Int. Ed. Engl.* **1985**, *24*, 786.

(26) Liu, Z.; Frasconi, M.; Lei, J.; Brown, Z. J.; Zhu, Z.; Cao, D.; Iehl, J.; Liu, G.; Fahrenbach, A. C.; Botros, Y. Y.; Farha, O. K.; Hupp, J. T.; Mirkin, C. A.; Stoddart, J. F. *Nat. Commun.* **2013**, *4*, 1855.

(27) (a) Smaldone, R. A.; Forgan, R. S.; Furukawa, H.; Gassensmith, J. J.; Slawin, A. M. Z.; Yaghi, O. M.; Stoddart, J. F. *Angew. Chem., Int. Ed.* **2010**, *49*, 8630. (b) Gassensmith, J. J.; Furukawa, H.; Smaldone, R. A.; Forgan, R. S.; Botros, Y. Y.; Yaghi, O. M.; Stoddart, J. F. *J. Am. Chem. Soc.* **2011**, *133*, 15312. (c) Han, S.; Wei, Y.; Valente, C.; Forgan, R. S.; Gassensmith, J. J.; Smaldone, R. A.; Nakanishi, H.; Coskun, A.; Stoddart, J. F.; Grzybowski, B. A. *Angew. Chem., Int. Ed.* **2011**, *50*, 276. (d) Forgan, R. S.; Smaldone, R. A.; Gassensmith, J. J.; Furukawa, H.;

Cordes, D. B.; Li, Q.; Wilmer, C. E.; Botros, Y. Y.; Snurr, R. Q.; Slawin, A. M. Z.; Stoddart, J. F. *J. Am. Chem. Soc.* **2012**, *134*, 406. (e) Furukawa, Y.; Ishiwata, T.; Sugikawa, K.; Kokado, K.; Sada, K. *Angew. Chem., Int. Ed.* **2012**, *51*, 10566. (f) Wei, Y.; Han, S.; Walker, D. A.; Fuller, P. E.; Grzybowski, B. A. *Angew. Chem., Int. Ed.* **2012**, *51*, 7435. (g) Wu, D.; Gassensmith, J. J.; Gouvêa, D.; Ushakov, S.; Stoddart, J. F.; Navrotsky, A. *J. Am. Chem. Soc.* **2013**, *135*, 6790. (h) Han, S.; Wei, Y.; Grzybowski, B. A. *Chem. - Eur. J.* **2013**, *19*, 11194. (i) Yoon, S. M.; Warren, S. C.; Grzybowski, B. A. *Angew. Chem., Int. Ed.* **2014**, *53*, 4437. (j) Gassensmith, J. J.; Kim, J. Y.; Holcroft, J. M.; Farha, O. K.; Stoddart, J. F.; Hupp, J. T.; Jeong, N. C. *J. Am. Chem. Soc.* **2014**, *136*, 8277. (k) Liu, Z.; Stoddart, J. F. *Pure Appl. Chem.* **2014**, *86*, 1323. (l) Bernini, M. C.; Fairen-Jimenez, D.; Pasinetti, M.; Ramirez-Pastor, A. J.; Snurr, R. Q. *J. Mater. Chem. B* **2014**, *2*, 766. (m) Michida, W.; Ezaki, M.; Sakuragi, M.; Guan, G.; Kusakabe, K. *Cryst. Res. Technol.* **2015**, *50*, 556. (n) Smith, M. K.; Angle, S. R.; Northrop, B. H. *J. Chem. Educ.* **2015**, *92*, 368. (o) Holcroft, J. M.; Hartlieb, K. J.; Moghadam, P. Z.; Bell, J. G.; Barin, G.; Ferris, D. P.; Bloch, E. D.; Algaradah, M. M.; Nassar, M. S.; Botros, Y. Y.; Thomas, K. M.; Long, J. R.; Snurr, R. Q.; Stoddart, J. F. *J. Am. Chem. Soc.* **2015**, *137*, 5706. (p) Hartlieb, K. J.; Holcroft, J. M.; Moghadam, P. Z.; Vermeulen, N. A.; Algaradah, M. M.; Nassar, M. S.; Botros, Y. Y.; Snurr, R. Q.; Stoddart, J. F. *J. Am. Chem. Soc.* **2016**, *138*, 2292. (q) Li, H.; Hill, M. R.; Huang, R.; Doblin, C.; Lim, S.; Babarao, R.; Hill, A.; Falcaro, P. *Chem. Commun.* **2016**, *52*, 5973.

(28) Ding, N.; Kanatzidis, M. G. *Nat. Chem.* **2010**, *2*, 187.

(29) McNulty, D. T. *Mining Magazine* **2001**, *184*, 256.

(30) (a) Vieira, R. *J. Cleaner Prod.* **2006**, *14*, 448. (b) Marcos, D. G.; Shikazono, N. *Int. J. Appl. Environ. Sci.* **2011**, *6*, 237. (c) Syed, S. *Hydrometallurgy* **2012**, *115−116*, 30.

(31) Norgate, T.; Haque, N. *J. Cleaner Prod.* **2012**, *29−30*, 53.

(32) Müezzinoğlu, A. *Crit. Rev. Environ. Sci. Technol.* **2003**, *33*, 45.

(33) Veiga, M. M.; Nunes, D.; Klein, B.; Shandro, J. A.; Velasquez, P. C.; Sousa, R. N. *J. Cleaner Prod.* **2009**, *17*, 1373.

(34) Cui, J.; Zhang, L. *J. Hazard. Mater.* **2008**, *158*, 228.

DOI: 10.1021/jacs.6b04986
J. Am. Chem. Soc. 2016, 138, 11643−11653